Journal of Power Sources 241 (2013) 654–659

Contents lists available at SciVerse ScienceDirect

Journal of Power Sources

journal homepage: www.elsevier.com/locate/jpowsour

Short communication

A highly active anode functional layer for solid oxide fuel cells based on proton-conducting electrolyte $BaZr_{0.1}Ce_{0.7}Y_{0.2}O_{3-\delta}$

Xiuling Zhang [a,*], Yu'e Qiu [a], Feng Jin [b], Feng Guo [a], Yulan Song [a], Baoyong Zhu [a]

[a] Key Laboratory of Coordination Chemistry and Functional Materials in Universities of Shandong, Dezhou University, Shandong 253011, PR China
[b] Department of Physics, Dezhou University, Shandong 253011, PR China

HIGHLIGHTS

- A highly active anode functional layer was employed to compose a quad-layer button fuel cell.
- A stable proton conductor was used as electrolyte.
- The anode structure configuration was optimized.
- Anodic interface was evaluated by electrochemical characterization.
- The cell performances were significantly improved at low temperatures.

ARTICLE INFO

Article history:
Received 5 February 2013
Received in revised form
29 April 2013
Accepted 5 May 2013
Available online 13 May 2013

Keywords:
Solid oxide fuel cell
Anode
Functional layer
Polarization resistance

ABSTRACT

Extensive works have been performed to diminish cathode polarization for proton-conducting electrolyte based solid oxide fuel cells (SOFCs) while not much attention is paid to functional anode for improving electrochemical reaction at three-phase-boundaries (TPB). In this work, a highly active anode functional layer (FL) synthesized by a modified combustion method was employed to significantly elevate the cell performance at intermediate operation temperatures (550–650 °C). The effects of anode structure configuration, FL powder size and thickness on power outputs and electrode polarization were investigated. A maximum power density of 489 mW cm^{-2} and a low electrode polarization resistance of 0.37 Ω cm^2 were achieved at 650 °C, indicating fuel gas transport and hydrogen oxidation reaction at TPB sites largely contribute to total cell resistance which could be effectively diminished by optimization of anodic interface environment with the adoption of highly active anode powders.

1. Introduction

Proton conducting solid oxide fuel cells (SOFC) have attracted much attention in recent years due to the advantages compared to conventional oxide-ion based SOFC, e.g., low activation energy for proton transport and high energy conversion efficiency [1–4]. Many perovskite (ABO_3) oxides show high proton conductivity in a wet atmosphere. One of the major challenges for this type of proton conductor is a proper compromise between conductivity and chemical stability [5–8]. Zuo et al. developed a stable and effective perovskite-type barium cerate with co-doping of yttrium and zirconium, $BaZr_{0.1}Ce_{0.7}Y_{0.2}O_3$ (BZCY) that exhibited both adequate proton conductivity as well as sufficient chemical and thermal stability over a wide range of conditions relevant to fuel cell operation [9]. Since then, much attention has been focused on improving the cell performance, especially the development of proper cathode materials because the cathode polarization losses dominate the total cell resistance [10–15]. Extensive works have been performed to effectively diminish the polarization resistance at low operation temperatures. The cathode materials and catalysis mechanism have been reviewed by R. Peng et al. [16]. In fact, anode is a critical component in SOFCs, responsible for facilitating the oxidation of the fuel and transport of electrons from reaction TPB to external circuit. Typically, anode consists of a three-phase percolating composite of nickel, an oxide electrolyte and the pore space [17] and the most commonly used nickel–zirconia cermet anodes display excellent catalytic properties and good current collection, which theoretically causes negligible polarization loss [18]. However, there are two factors significantly contributing to the losses of electrode polarization due to structure design and fabrication process: (i) pore structure, which affects gas transportation and conversion; (ii) porosity, which is closely related to material

* Corresponding author. Tel.: +86 534 8985835.
E-mail address: xiulingzhang123@163.com (X. Zhang).

0378-7753/$ – see front matter © 2013 Elsevier B.V. All rights reserved.
http://dx.doi.org/10.1016/j.jpowsour.2013.05.002

Table 1
A schematic of anode structural configuration of different cells.

Sample	Structural configuration
Cell-A	NiO–BZCY substrate/NiO–BZCY functional layer/BZCY electrolyte
Cell-B	Porous NiO–BZCY anode substrate/BZCY electrolyte
Cell-C	Starch-free NiO–BZCY anode/BZCY electrolyte

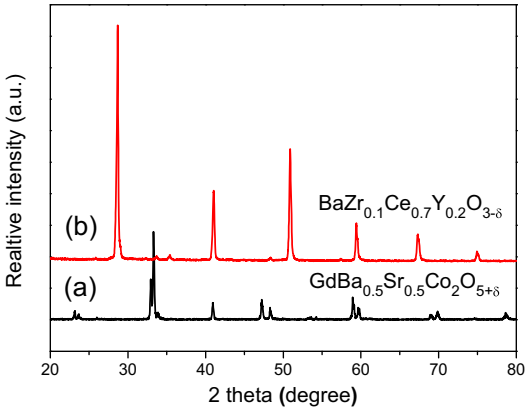

Fig. 1. XRD diffraction patterns for (a) the layered $GdBa_{0.5}Sr_{0.5}Co_2O_{5+\delta}$ (GBSC) perovskite powders and (b) $BaZr_{0.1}Ce_{0.7}Y_{0.2}O_{3-\delta}$ (BZCY) powders.

properties as well as mass transfer. The combination of both parameters can also effectively affect the structure of electrode interface which electrochemically determines the TPB reaction condition. The anode/electrolyte interface is a critical reaction area since only partial oxygen ions can be conducted to extended anode substrate and react with protons. Generally, the gas pores are partially produced by mixing organic particles, e.g. starch or graphite [19], which are removed in sintering process and consequently leave in-situ open pores. In addition, the reduction of NiO particles to Ni can also increase the porosity due to the reduction of particle volume. In practical anode fabrication process, however, the homogeneous pores distributed in whole anode would be bound to extend to the anode/electrolyte interfaces, resulting in the disconnection between two layers to some extent. The inter-lamination separation can lead to high ohmic resistances and eventually decrease the anode performance. In this work, a highly active anode functional layer is employed to improve the anodic interface for promotion of the TPB reaction and anode performance by structure optimization and application of electrochemically catalytic anode powders. The effects of anode configuration, FL powder size and thickness on electrode polarization and power outputs were investigated in detail.

2. Experimental

2.1. Materials synthesis and fuel cell preparation

The functional anode NiO–$BaZr_{0.1}Ce_{0.7}Y_{0.2}O_{3-\delta}$ (NiO–BZCY) powders were synthesized by Pechini method with citrate and ethylenediamine tetraacetic acid (EDTA) as parallel complexing agents. Y_2O_3 was dissolved in nitric acid first, and stoichiometric amounts of $Ni(NO_3)_2\cdot 6H_2O$, $Ba(NO_3)_2\cdot 9H_2O$, $Ce(NO_3)_3\cdot 6H_2O$ and $Zr(NO_3)_4\cdot 4H_2O$ were then dissolved into EDTA aqueous solution. The final molar ratio of EDTA, metal ions and citric acid was controlled at 1.5:1:1. The solution was heated under stirring to ignite. The powders were collected and calcined in air at 1000 °C for 3 h to form the composite anode. The morphology of the powders was observed by transmission electron microscope (TEM). The details of synthesis of electrolyte BZCY and cathode $GdBa_{0.5}Sr_{0.5}Co_2O_{5+\delta}$ (GBSC) powders can be found at somewhere else [9,17]. The crystal structure of prepared BZCY and GBSC powders was studied with the powder X-ray diffraction by Cu-Kα radiation.

The anode-supported quad-layer button cells were fabricated by a conventional dry-pressing/co-firing method. The mixture of commercial NiO, BZCY and starch (3:2:1 in weight) was pre-pressed at 200 MPa to form an anode substrate, and then the loose anode functional layer was pressed onto the substrate. Finally BZCY powders synthesized above were uniformly distributed onto the anode substrate, co-pressed at 250 MPa, and subsequently co-sintered at 1350 °C for 5 h to obtain the tri-layer cells of NiO–BZCY substrate/NiO–BZCY functional layer/BZCY electrolyte (briefly cell-A) as shown in Table 1. For comparison, the cell with only porous NiO–BZCY anode substrate (briefly cell-B) and the cell with starch-free anode (briefly cell-C) were also fabricated. The as-synthesized GBSC cathode powders by the same process were calcined at 1000 °C for 3 h. The composite cathode slurry was prepared by mixing 25 wt% BZCY and 75 wt% GBSC with a 6 wt% ethyl cellulose–terpineol binder. The slurry was painted on electrolyte films of cell A, B and C respectively, which were then sintered at 1000 °C for 3 h to form single cells. The electrode active area was about 0.24 cm^2.

2.2. Characterization of electrochemical performance and microstructure

After being sealed onto alumina tube, the single cells (A, B and C) were tested in an electrical furnace with humidified hydrogen as fuel and the static air as oxidant, respectively. The flow rate of fuel was controlled at 20 ml min^{-1}. The power outputs and AC impedance spectroscopy were tested at temperatures from 500 to 650 °C. The frequency range was 0.1–10^5 Hz with the signal amplitude of 10 mV. The morphology of the single cell after the electrochemical tests was characterized by a scanning electron microscope (SEM).

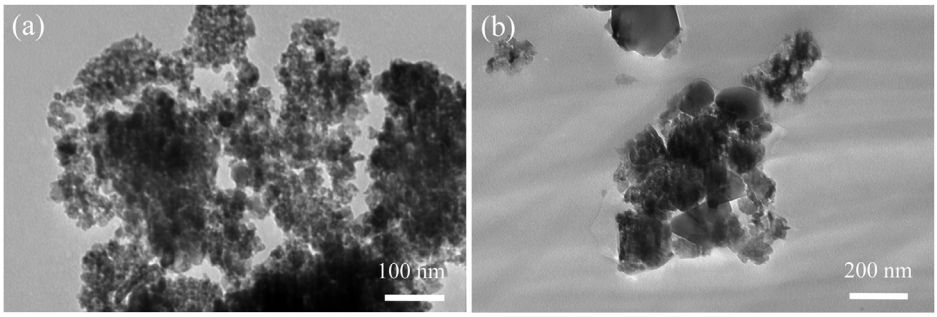

Fig. 2. TEM image for (a) NiO–BZCY composite functional anode powders synthesized by modified Pechini method and (b) commercial NiO and BZCY mixture powders.

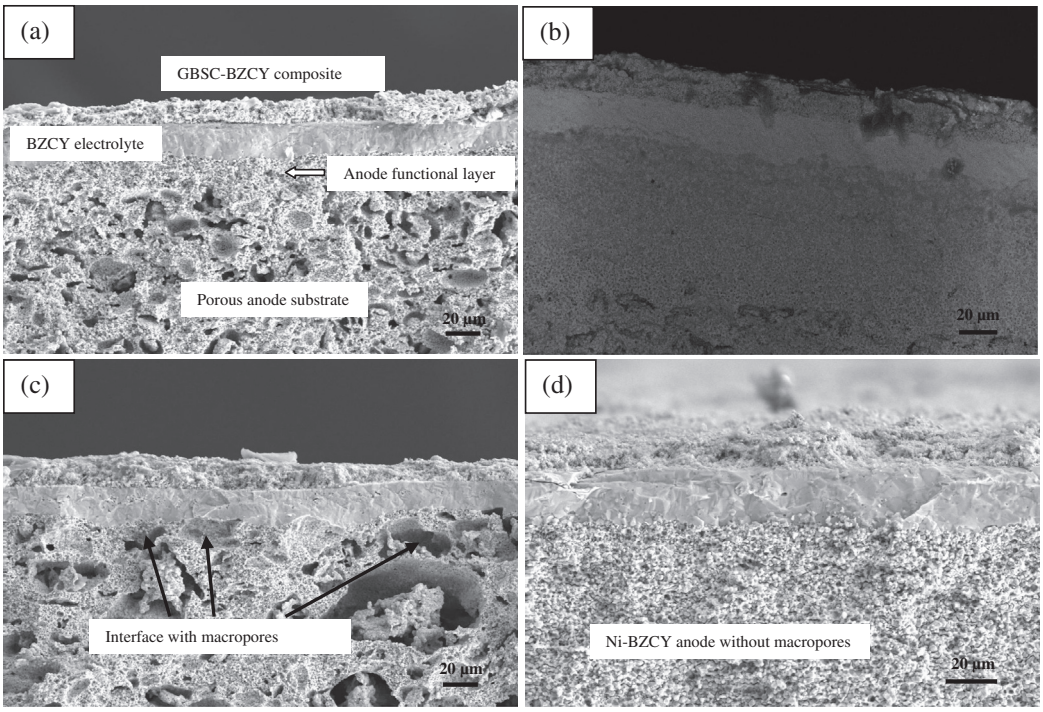

Fig. 3. The SEM images of (a) cross-section view of cell-A with a 20 μm-thick BZCY membrane and anode FL after testing; (b) backscattered image; (c) cell-B without FL and (d) cell-C with only FL.

3. Results and discussion

As shown in Fig. 1a, the cathode GBSC powders after calcined at 950 °C for 3 h exhibit a typical layered perovskite phase without any other peaks attributable to possible impurities [20]. Fig. 1b presents the XRD spectra of BZCY electrolyte calcined at 1000 °C for 3 h. The diffraction peaks were identical with standard peaks of barium cerate, which were also identical with those of BZCY in other literature [9].

Fig. 2 shows the TEM images for the morphology of NiO–BZCY composite powders synthesized by modified Pechini method and mixed powders of BZCY by solid-state reaction method and

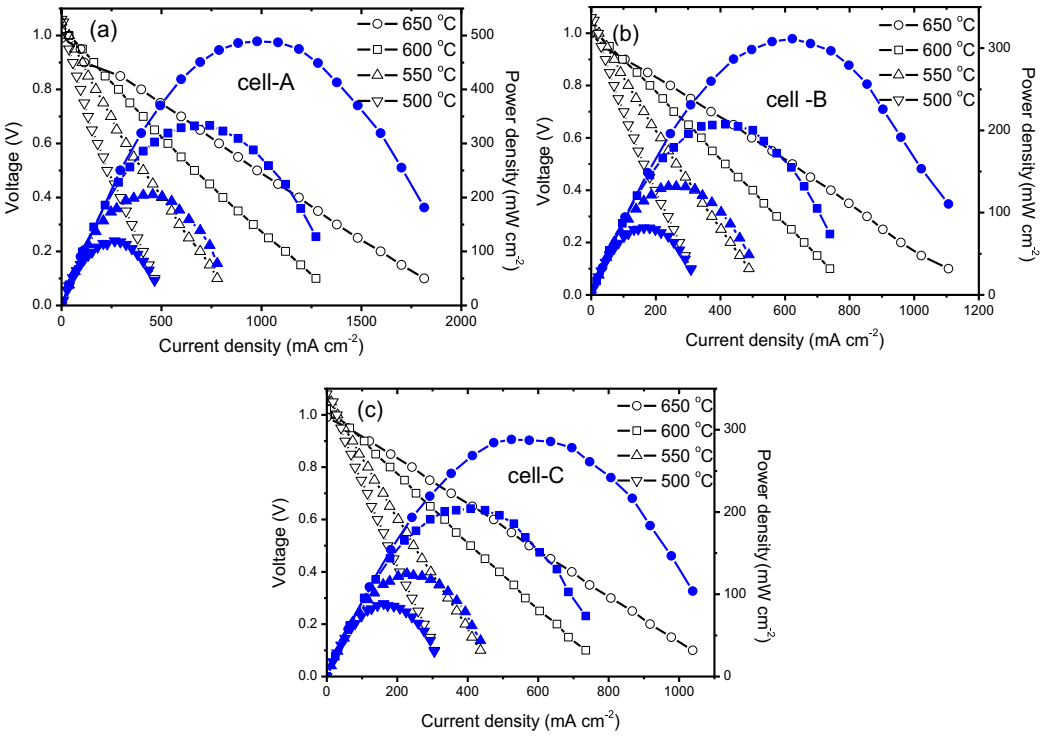

Fig. 4. Electrochemical performance of (a) cell-A; (b) cell-B and (c) cell-C under humidified hydrogen atmosphere at different temperatures.

commercial NiO. The grain size of composite anode in Fig. 2a is uniform at about 20 nm after calcined at 1000 °C for 3 h. When the nanoparticles are utilized as a functional layer between anode substrate and electrolyte, potentially it could effectively avoid the macro-pores at the interface and promote the catalytic ability, which will be discussed later. In Fig. 2b, as we can see, NiO particles were apparently much larger and it can be expected that contracted NiO particles after reduced by hydrogen will lead to formation of large gas pores at the interfaces in the electrochemical test process, resulting in significant decrease of power density.

Fig. 3 shows the cross-section view of single cell A (NiO–BZCY porous substrate/NiO–BZCY functional layer/BZCY), cell B (anode only with porous NiO–BZCY substrate) and cell C (anode only with active powders) after electrochemical test. As can be seen, the BZCY electrolytes were about 20 μm in thickness, quite dense and adhered very well to the GBSC layer, indicating that the cell performances would not come from the difference of the electrolyte thickness. In the quad-layer assembly cell-A (Fig. 3a), macro-gas pores were generated by in-situ removal of starch particles in the sintering process and distributed all over the bottom porous anode substrate. Obviously, these macro-pores are favorable for the fuel gas transporting to critical TPB area. The anode functional layer (FL) made of highly active NiO–BZCY powders constitutes a significant component between electrolyte and anode substrate, which affects the anodic catalysis and interface resistance. This compact layer without observable gas pores has highly effective contact with electrolyte, which can essentially enhance the length of the three-phase boundary (TPB), where protons transfer to cathode side through functional layer/electrolyte interface and electrolyte bulk. The two phases (NiO and BZCY) with homogeneous distribution indicated that the modified Pechini method could obtain nano-sized catalytic composite powders, which certainly benefits the cell performance (backscattered image in Fig. 3b). Contrarily, the cell B without functional layer has a poor anode/electrolyte interface with massive gaps, which substantially decrease the contact area of proton generation layer and proton transportation layer (Fig. 3c). The monolayer porous anode substrate with continuous macro-pores distribution is bound to form the contact of electrolyte with the pores, leading to the increase of ohmic resistance, which seriously affects the power outputs. Fig. 3d shows the anode with only highly active NiO–BZCY as substrate. The lack of gas pores in anode substrate will inhibit the fuel gas transit which will clearly increase the concentration polarization. In all cells, the BZCY electrolyte is sufficiently dense and thickness is constantly about 20 μm for evaluating the differences between the three types of cells equally.

The electrochemical performance of cell A, B and C with different anodes is tested at different temperature with humid hydrogen as fuel and static air as oxidant respectively in order to evaluate the effect of the anode microstructure on cell performance. As we can see from Fig. 4b that the maximum power density (P_{max}) of cell B without functional layer was only 311 mW cm^{-2} at 650 °C. For cell C with less porous anode, the P_{max} was also only 288 mW cm^{-2} at 650 °C (Fig. 4c). The current densities at 0.1 V for both cells were 1106 mA cm^{-2} and 1038 mA cm^{-2}, respectively. For cell A, the P_{max} was significantly improved to 489 mW cm^{-2} (Fig. 4a) when the functional anode layer was employed. The results could be explained by the improvement of anode configuration which is dominative in the anode polarization. For cell B, the low current density is primarily caused by the macro-pores inhibiting the complete contact between anode and electrolyte; consequently significantly decrease the TPB reaction sites accompanying the transportation of electron and ions. Lin et al. reported that the poor condition of the anode/electrolyte interface (based on oxide ion $Sm_{0.2}Ce_{0.8}O_{1.9}$ (SDC) electrolyte) would certainly reduce the length of TPB, where the electrochemical reaction takes place [21]. Usually the monolayer porous and uniform anode cannot prevent the formation of macro-pores, however, the anode without any starch as pore maker in sintering process can cause another problem even though it has good interface. The less porosity (~23%) caused the difficulty that hydrogen could not pass to the TPB interface throughout the thick substrate without sufficient pores, which lead to low reaction rate between oxygen ions and protons. In cell C, the whole porosity is introduced by volume shrinkage of nickel oxide to metal nickel in anode reduction process. In general, this amount of pores is not sufficient for the gas transport. The results indicated that both cell B and cell C were not suitable anode structures for gas transport or TPB reaction. For cell A, the compromise between porous anode and relatively dense anode can possibly optimize proper anode structure configuration for gas transport as well as formation of good interface for electrochemical reaction, which were demonstrated by the significant increase of the P_{max} and high current density at 0.1 V. Meanwhile, it is noteworthy that the effect of the similar interface between the FL and anode substrate with sharp porosity change as that in cell A didn't affect anode reaction too much. This is mainly due to homogeneous components in both layers in which the high electronically conductive and catalytically active nickel and proton conductive BZCY play critical roles in cell performance. For the later interface in cell A, the heterogeneous conductive layers (proton from BZCY and electron from nickel in anode) belong to two

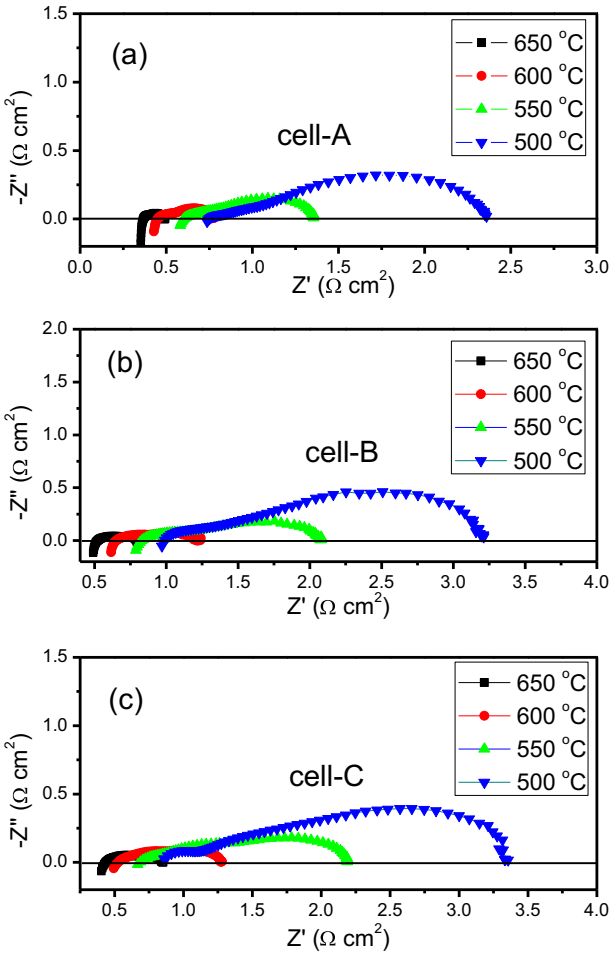

Fig. 5. Impedance spectra of (a) cell-A; (b) cell-B and (c) cell-C measured under open-circuit conditions at different temperatures.

different material systems but connect with each other where the protons are catalyzed by nickel and transported through electrolyte membrane. Therefore, the cell performance is intrinsically sensitive to contact condition in whole interface.

In order to evaluate the effect of anode/electrolyte interface on the cell performance, the electrochemical impedance spectra (EIS) were measured under open-circuit condition to obtain the cathode polarization contributing to the total cell resistance, which are shown in Fig. 5. The total electrode polarization resistances can be readily obtained from the difference between the high-frequency and low-frequency intercepts of impedance loop with the real axis where high-frequency and low-frequency intercepts of impedance loop with the real axis correspond to ohmic resistance (R_o) and total resistance (R_t). For cell B, the R_o was 0.52 Ω cm^2 at 650 °C, 0.65 Ω cm^2 at 600 °C and 0.83 Ω cm^2 at 550 °C, respectively (Fig. 5b). When functional layer is applied, the R_o of cell A was obviously improved to 0.37 Ω cm^2 at 650 °C, 0.45 Ω cm^2 at 600 °C and 0.6 Ω cm^2 at 550 °C (Fig. 5a). The less porous FL promotes the contact between electrolyte and substrate and makes the electrons and protons transportations more efficient. Meanwhile, the R_p was also reduced greatly because of improved interface, which is related with highly active FL powder used in fabrication procedure. In Lin et al.'s work, the anode FL of Ni-SDC also effectively improved the interface with greatly decreased cell resistance. The results also demonstrated the addition of active anode FL is an effective way to improve electrode interface by minimizing ohmic resistance from macro-pores. Meanwhile, however, the poor performance of cell C (R_o = 0.43 Ω cm^2, R_p = 1.6 Ω cm^2 at 650 °C, Fig. 5c) indicated porosity is another adjustable parameter with effect on gas transportation. Therefore, the effect of anode FL thickness on the power outputs was investigated to obtain the reasonable structure configuration. The thickness was controlled by the weight of the composite powder of NiO–BCZY with mole ratio of 6:4 in the dry-pressing procedure. As we can see from cross-section views (Fig. 6), the cells have the same thickness of the electrolyte and cathode but different functional anode layers (30 μm, 50 μm and 260 μm, respectively) adhered to both electrolyte and anode substrate layers well. The electrochemical performances of the cells were shown in Fig. 7 to compare the peak power density at 650 °C with the same hydrogen flow rate of 30 ml min^{-1}. The P_{max} decreased by 37% from 489 mW cm^{-2} to 308 mW cm^{-2} as the FL increased to 260 μm. The EIS results also showed linear increase of ohmic

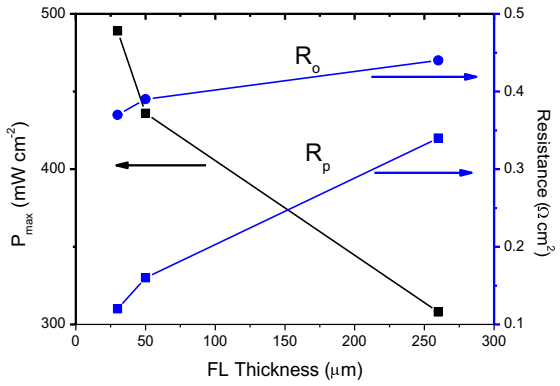

Fig. 7. The maximal power densities (P_{max}), R_o and R_p change with the FL thickness.

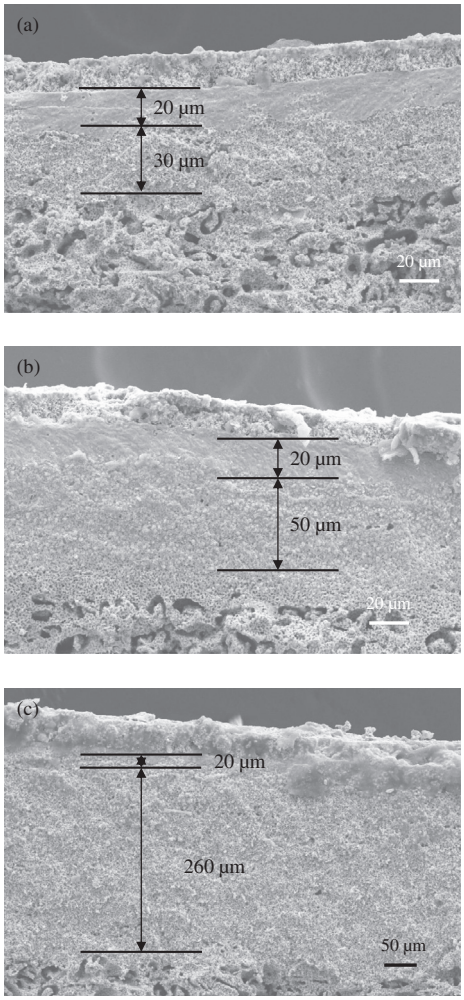

Fig. 6. The SEM images of tri-layer button cells with different thickness FL: (a) 30 μm; (b) 50 μm and (c) 260 μm.

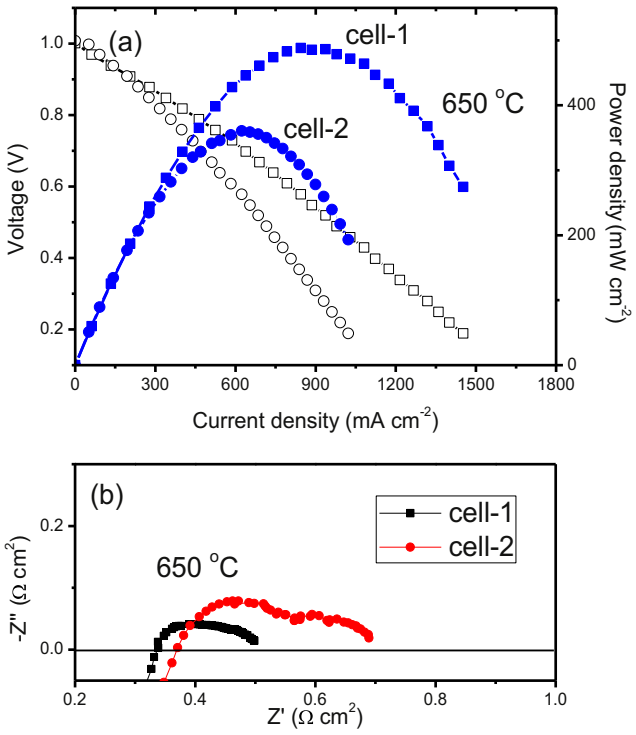

Fig. 8. (a) The performances of cell-1 and cell-2 and (b) impedance spectra of cell-1 and cell-2 at 650 °C.

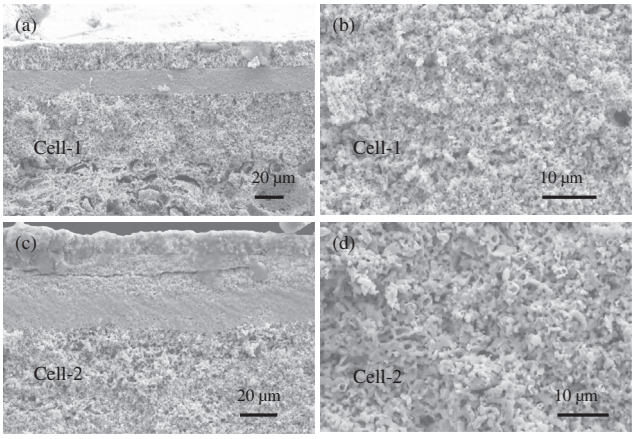

Fig. 9. The cross-section SEM images of (a) cell-1 with FL fabricated from 20 nm anode powder after test and (b) porous FL with fine grain; (c) cell-2 with FL prepared from 1 μm anode powder and (d) FL magnification view.

resistance and electrode interfacial resistance by 18.9% and 183% respectively. From the view of mass and charge transfer, the FL can prevent the gas moving to the effective TPB area which is restricted to limited interface. However, due to the present technical limitation of fabricating the thinner functional anode layer, the range of (5–20 μm) was not studied and further optimization of FL thickness is still needed to reach the ideal value. Since fuel transport essentially affects interfacial resistance, another critical factor of FL powder size was also investigated to understand the relation between anode reaction rate and the size. Due to the low conductivity of BZCY and thick and porous anode substrate, the protons formed at the anode substrate have low transfer rate to the TPB area, which requires FL contribute more to hydrogen oxidation. Therefore, the active anode powders with average diameter size of 20 nm synthesized by combustion method were employed to obtain 30 μm thick FL (cell-1). For comparison, the single cell with FL (powder diameter of 1 μm) was also fabricated (cell-2). As we can see from Fig. 8a, the P_{max} for cell-1 reached 488 mW cm^{-2} at 650 °C and P_{max} of cell-2 was only 360 mW cm^{-2}. The electrode polarization resistance of cell-1 was 0.17 Ω cm^2, smaller than that of cell-2 (0.32 Ω cm^2, Fig. 8b). From the cross-section view in Fig. 9, after sintering at 1350 °C for 5 h, the grain size of FL using Ni–BZCY nanoparticles was much smaller than that of cell-2. Obviously, the nano-sized powders still keep relatively smaller grain, which is favorable to anode reaction. Meanwhile, the FL powders can also promote anode substrate contraction for electrolyte densification. The linear shrinkage of diameter in cell-1 reached 26%, much bigger than that of cell-2 (~16%). The results indicated that the thickness and powder size of FL have significant effect on electrode polarization based on proton-conductor electrolyte SOFCs.

4. Conclusions

The electrochemically active NiO–BZCY mixed electronic–protonic conductive powders were investigated as anode functional layer which was demonstrated to improved electrode resistance significantly due to the optimized anode/electrolyte TPB interface and excellent H_2 oxidation activity of nano-sized anode powder. The effect of FL thickness and particle size on the anode polarization was studied by comparing with conventional anode substrate without FL on power densities and EIS results. After structural optimization, the FL made of highly active NiO–BZCY powders constitutes a critical component between electrolyte and anode substrate, and the P_{max} reached 489 mW cm^{-2} and a low electrode polarization resistance of 0.12 cm^2 was achieved at 650 °C.

Acknowledgment

This research was supported by National Nature Science Funding of China (20971018), Natural Science Fundation of Shandong Province (ZR2010BL010) and Technology Development Project of Shandong Province (2010GWZ20251).

References

[1] B.C.H. Steele, A. Heinzel, Nature 414 (2001) 45.
[2] Q. Ma, R. Peng, L. Tian, G. Meng, Electrochem. Commun. 8 (2006) 1791.
[3] A.F. Sammells, R.L. Cook, J.H. White, J.J. Osborne, R.C. MacDuff, Solid State Ion. 52 (1992) 111.
[4] K. Kreuer, Annu. Rev. Mater. Res. 33 (2003) 333.
[5] N. Bonanos, K. Knight, B. Ellis, Solid State Ion. 79 (1995) 161.
[6] S. Gopalan, A. Virkar, J. Electrochem. Soc. 140 (1993) 1060.
[7] F. Zhao, Z. Wang, M. Liu, L. Zhang, C. Xia, F. Chen, J. Power Sources 185 (2008) 13.
[8] S. Tao, J. Irvine, Adv. Mater. 8 (2006) 1581.
[9] C. Zuo, S. Zha, M. Liu, M. Hatano, M. Uchiyama, Adv. Mater. 18 (2006) 3318.
[10] X. Zhang, M. Jin, J. Power Sources 195 (2010) 1076.
[11] S. McIntosh, J. Vente, W. Haije, D. Blank, H. Bouwmeester, Chem. Mater. 18 (2006) 2187.
[12] H. Ding, B. Lin, X. Liu, G. Meng, Electrochem. Commun. 10 (2008) 1388.
[13] K. Yoon, W. Huang, G. Ye, S. Gopalan, U. Pal, D. Seccombe, J. Electrochem. Soc. 154 (2007) B389.
[14] L. Zhang, S. Jiang, W. Wang, Y. Zhang, J. Power Sources 170 (2007) 55.
[15] A. Grimaud, F. Mauvy, J.M. Bassat, S. Fourcade, L. Rocheron, M. Marrony, J.C. Grenier, J. Electrochem. Soc. 159 (6) (2012) B683.
[16] R. Peng, T. Wu, W. Liu, X. Liu, G. Meng, J. Mater. Chem. 20 (2010) 6218.
[17] A. Atkinson, S. Barnett, R. Gorte, J. Irvine, A. Mcevoy, M. Mogensen, S. Singhal, J. Vohs, Nat. Mater. 3 (2004) 17.
[18] L. Bi, E. Fabbri, Z. Sun, E. Traversa, Energy Environ. Sci. 4 (2011) 1352.
[19] X. Zhang, M. Jin, J. Sheng, J. Alloys Compd. 496 (2010) 241.
[20] J. Kim, M. Cassidy, J. Irvine, J. Bae, J. Electrochem. Soc. 156 (2009) B682.
[21] B. Lin, J. Chen, Y. Ling, X. Zhang, Y. Jiang, L. Zhao, X. Liu, G. Meng, J. Power Sources 195 (2010) 1624.